Journal of Materials Chemistry A

PAPER

View Article Online
View Journal | View Issue

Cite this: J. Mater. Chem. A, 2019, 7, 12616

Electroforming of a metal–organic framework on porous copper hollow fibers†

Özlem H. Demirel, Timon Rijnaarts, Patrick de Wit, Jeffery A. Wood and Nieck E. Benes *

Porous copper hollow fibers have been used, for the first time, as both a support structure and a metal source for preparing thin metal–organic framework (Cu-BTC) films *via* a fast, facile and direct electrochemical route. The focus is on the effects of the presence of a supporting electrolyte and the magnitude of the applied electrical potential on the formation and the morphology of the films. In the absence of a supporting electrolyte, and at low potential, more uniform films with smaller particles are obtained. This is attributed to the more pronounced electric-field driven mass transport of the organic ligand from the liquid bulk towards the surface of the electrode combined with the slower dissolution of copper due to the lower overpotentials. In the presence of a supporting electrolyte the ligand transport is much slower and copper dissolution is higher due to higher overpotentials; this results in the formation of less homogeneous films and the growth of metal–organic framework crystals in the liquid bulk. The localized formation of thin metal–organic framework films on metal porous hollow fibers with high surface area to volume ratio is an important step towards various applications, including membranes, microfluidic devices, sensors and heterogeneous catalysts.

Received 23rd November 2018
Accepted 14th April 2019

DOI: 10.1039/c8ta11296g

rsc.li/materials-a

1 Introduction

Metal–organic frameworks (MOFs) are hybrid materials consisting of inorganic metal centers connected by organic linkers. This nature gives MOFs synergetic properties of both inorganic and organic porous materials. MOFs have been studied for many different applications over the past decade due to their high surface area and porosity, relatively good thermal and chemical stability, designable framework, flexibility, sorption capacities, and functionalizability.[1–6] For example, MOF thin films have attracted attention for application in separations, sensors, electric devices, and catalytic coatings.[7–11] Efforts towards controlling MOFs' localized synthesis, morphology and thickness have become crucial for these applications. MOF films can be prepared by multiple methods, including *in situ* and secondary growth,[12] dip coating,[13] layer by layer growth,[14] and electrochemical fabrication methods.[15] After the electrochemical fabrication method was first developed for MOF powder synthesis by BASF in 2005, preparation of MOF films *via* an electrochemical route has also been explored.[16,17] The electrochemical method has a number of advantages *versus* other techniques. First, it is a facile technique that offers the advantages of using lower temperatures than those needed for traditional methods. Second, by using a pure metal source instead of a metal salt, the formation of undesirable by-products, such as nitrates, is prevented.[18] Third, the time required for electrochemical synthesis is typically on the order of minutes while for other approaches it can be hours or days.[19]

Until now, 14 different MOFs have been electrochemically synthesized as thin films.[20] Among them, Cu-BTC ($Cu_3(BTC)_2$, HKUST-1, BTC = benzene-1,3,5-tricarboxylate) is the most studied electrochemically synthesized type of MOF in the literature. There are different electrochemical fabrication techniques, including anodic oxidation,[17–19,21–25] cathodic deposition,[26,27] galvanic displacement,[28] and electrophoretic deposition.[29,30] Anodic oxidation is the most common and the most straightforward technique. In this method, a working electrode (anode) is used both as a metal source and a support for the MOF films. By applying a potential difference between the working electrode and a counter electrode, metal ions are released and they react with the organic linker available in the synthesis solution and the MOF film is formed. Under the right synthesis conditions the formation of the MOF occurs on the surface of the working electrode and a thin film is formed. Often, a supporting electrolyte is used to enhance the conductivity of the organic solution due to its high resistivity.[19]

Efforts have been made to investigate the crystallization mechanism, the reaction mechanism and the factors affecting the MOF film thickness and quality. It has been shown that dense and thin MOF films can be prepared on a partially oxidized support without damaging it by controlling the applied

Membrane Science and Technology Cluster, Faculty of Science and Technology, MESA+ Institute for Nanotechnology, University of Twente, P. O. Box 217, 7500 AE, Enschede, The Netherlands. E-mail: n.e.benes@utwente.nl

† Electronic supplementary information (ESI) available. See DOI: 10.1039/c8ta11296g

potential and time and using a supporting electrolyte.[18] In the anodic dissolution method, MOF formation consists of four different steps: (i) initial nucleation, (ii) growth of islands, (iii) intergrowth and (iv) detachment.[25] The reaction mechanism of the synthesis has been found to be a two-step oxidation mechanism.[24] First, the presence of oxygen and water initiates the oxidation of Cu^0 to Cu^{+1} as the form in Cu_2O. Second, Cu_2O in the presence of an organic linker solution leads to the formation of $Cu_3(BTC)_2$. Cyclic voltammetry (CV) of Cu-BTC synthesis has been studied using Au (111) as a substrate to shed light on the mechanism.[31] After the deposition of copper on the Au surface, the interaction between the organic linker and copper in ethanol has been investigated. The oxidation of copper shifted to higher potentials due to the adlayer (adsorbed layer) of the organic linker on the copper surface. This may explain the good attachment of MOFs on the copper surface. It is also found that Cu oxidation occurs at low potentials (0.18 V in the presence of BTC) whereas a very large range of applied potentials have been used in the literature (0.5–25 V).[17,31] This can also be related to the use of a two-electrode or three-electrode electrochemical cell. In a three-electrode cell, the applied potential between the working and reference electrode can be controlled precisely, whereas in a two-electrode cell it is not possible to know the exact potential applied to the working electrode since it is not *versus* a reference electrode.[15] Solutions suffer from high (ionic) resistivity due to the use of an organic solvent, which limits charge transport and thus electron transfer at the surface. In order to decrease the ohmic (resistance) drop in the solution and increase the efficiency of the synthesis, a supporting electrolyte is typically added to the synthesis solution. Some studies have found that the supporting electrolyte has a strong effect on the kinetics of the reaction.[18,32] This can cause some cracks or defects on the substrate and it has been found that MTBS (methyltributylammonium methyl sulfate), a supporting electrolyte commonly used in organic solutions, can be trapped in the pores of the MOF and cause a decrease in the pore volume and specific surface area.[33]

Up to now, there have been various studies to obtain MOF films on various copper supports such as plates, disks, meshes, beads and copper coated silicon wafers, using gold and glass carbon electrodes.[15,16,18,31,34–36] However, to the best of our knowledge, electrochemical deposition of MOFs directly on porous hollow fibers (HFs) has not been previously reported. HFs are attractive for many industrial applications due to their high surface area to volume ratio and easy scale-up features. Therefore, MOF HFs have gained interest as mixed matrix HF membranes,[37–39] MOF films coated onto polymeric HFs[40,41] or ceramic HFs incorporated with MOFs.[42] In this work, we have prepared Cu-BTC-coated Cu HFs *via* an electrochemical synthesis route. We show that electrochemical synthesis can be used for MOF film formation on the outer surface of metal HFs as a fast, simple and efficient direct synthesis technique. We investigated different synthesis conditions in order to obtain homogeneous, uniform and continuous MOF films and characterized based on the adhesion of layers, their thickness, and their particle size distribution.

2 Experimental

2.1 Preparation of Cu-BTC-coated Cu HFs

Cu-BTC-coated Cu HFs were prepared using a three-electrode electrochemical cell (Fig. 1). As a starting point, an adapted procedure of Van Assche, 2012, and Schäfer, 2016, with different substrates (*e.g.* copper mesh and copper plate) was followed.[18,24] A copper HF, with a wall thickness of *ca.* 0.25 mm, an inner diameter of *ca.* 1 mm and an average length of 10 cm, was used as a working electrode (WE) (Fig. 1(c)). The preparation of copper HFs *via* non-solvent induced phase separation is described in detail elsewhere.[43] A copper wire ($r = 0.23$ mm) was polished using 240 grit sandpaper and used as a counter electrode (CE). As a reference electrode (RE), a saturated calomel electrode (SCE) (from SI Analytics) was used.[44] All the reported electrical potential values were based on the standard hydrogen electrode (SHE). The synthesis mixture was prepared by adding the organic linker benzene-1,3,5-tricarboxylic acid (trimesic acid, BTC) (Sigma Aldrich, ≥95%) and the supporting electrolyte methyltributylammonium methyl sulfate (MTBS) (Santa Cruz Biotechnology, >98%) both with a concentration of 16 g L^{-1} into a mixture of purified ethanol (EtOH, ≥99.9%, EMSURE®) and water (H_2O, purified using a Milli Q system, Millipore) (EtOH : H_2O 65 : 35 v/v).

All the electrodes were placed in the solution. The cell was heated to 50 °C by immersing the assembly in a hot water bath. A PGSTAT204 potentiostat (Metrohm Autolab, B. V., The Netherlands) was used to apply a potential difference across the electrodes. For a given experiment, the desired potential was applied to the samples and synthesis was allowed to take place over a given time (30 minutes). The current was recorded during the synthesis and was reported as an average over time (Fig. S1† and Table 1). After the electrochemical synthesis, the MOF-HFs were rinsed in ethanol for 2 days followed by drying at ambient temperature for further analysis. The effect of the presence of the supporting electrolyte in the synthesis solution and the effect of the applied potential (0.5–5 V *vs.* SHE) were investigated. The Cu-BTC-coated Cu HF samples synthesized in the presence of the electrolyte and in the electrolyte-free solution were called E-(applied potential) and F-(applied potential), respectively.

2.2 Materials characterization

The Cu-BTC-coated Cu HFs were investigated using an SM-6010 (JEOL) scanning electron microscope equipped with an energy dispersive X-ray spectrometer (EDS). MOF thin layer deposition was essentially uniform on the HF surface, with only slight differences that may be attributed to the effect of the curvature of the HF and the local electric-field distribution. Consequently, in the analysis variations based on position were not considered. The cross-sections and the outer surface of fibers were sputtered with a 5 nm chromium coating (Quorum Q150T ES) prior to analysis. The XRD patterns of the samples were determined by powder X-ray diffraction (XRD) on a Bruker D2 PHASER operated at 10 mA and 30 kV using a CuKα source with a wavelength (λ)$\frac{1}{2}$ 1.54 Å at room temperature. Scans were

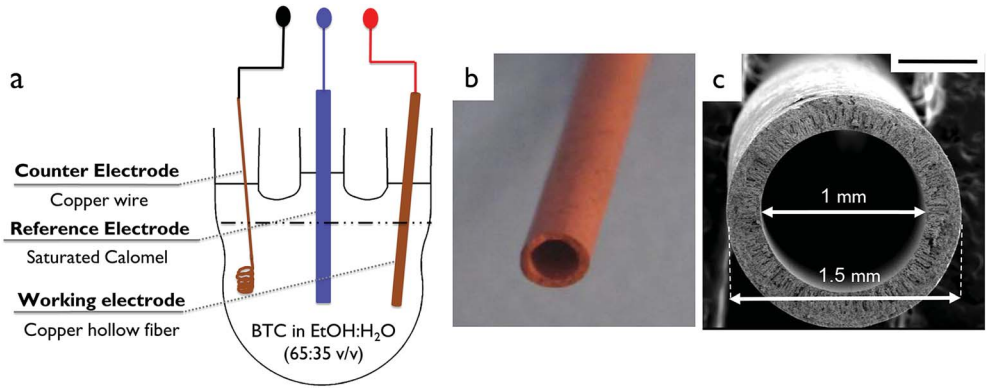

Fig. 1 (a) Schematic overview of the three-electrode cell. (b) Porous copper HF; (c) cross-sectional image of the copper HF. Scale bar, 500 μm.

carried out at variable angles, ranging from 5 to 50° with a 2θ step size of 0.02° and a scan speed of 1 s per step. The MOF sample for XRD analysis was obtained by scratching the outer surface of the fibers. Thermogravimetric analysis (TGA) was performed using a STA 449 F3 Jupiter (Netzch). Measurements were performed under 20 ml min^{-1} nitrogen flow and at a heating rate of 5 °C min^{-1}, starting from room temperature up to 800 °C. Temperature correction with the melting point standard and a blank correction with an empty cup were carried out prior to the measurements.

2.3 Particle size and film thickness analysis

Particle size and film thickness were determined by image analysis (ImageJ software) using outer surface and cross-sectional SEM images, respectively.[45] The particle size analysis was performed for each sample using at least two outer surface images and for more than 300 particles in total. The minimum threshold was set at 5 particles per bin (bins 0.2 μm in width), and bins containing fewer than this number were not included in the analysis. The particle size was fitted to a Gaussian distribution using least squares regression. The thickness of the MOF films was calculated by taking more than 10 measurements per cross-sectional SEM image. The mean particle size, the spread and thickness data are reported along with the standard error.

3 Results and discussion

Here, MOF film formation on the outer surface of the copper HF *via* an electrochemical route is investigated. We considered two cases: with and without a supporting electrolyte. In the first case, with the supporting electrolyte, electrical potential gradients in the bulk are reduced or negligible due to the higher conductivity of the synthesis solution. In the second case, larger electrical potential gradients can exist in the bulk which can favor the transport of charged species to and from the electrodes *via* electromigration. From the perspective of electrocrystallization, MOF film formation *via* an electrochemical method is a surface reaction that takes place in the electrical double layer (near the electrode surface). Partial oxidation of the copper HF support and transport of BTC in order to react and form the MOF layer are then the critical parameters controlling the properties of the MOF film.

3.1 Cu-BTC MOF film characterization

Fig. 2 shows that Cu-BTC MOF crystals with the typical octahedral shape were formed on the outer surface of the HF. In Fig. 3 the EDS data depict the atomic composition of the films, revealing the presence of a uniform Cu-BTC MOF structure containing both organic (C) and metal (Cu) components. The X-ray diffraction patterns of the MOF films that were prepared

Table 1 Results of Cu-BTC-coated Cu HF synthesis. Particle size analysis of the MOFs, determined by image analysis (by ImageJ software) of the SEM image at different magnifications (×1000 to ×7500). The thickness of MOF films – synthesized for 30 min for both sets of experiments (E and F) – was calculated by taking more than 10 measurements per cross-sectional SEM image at different magnifications (×500 to ×2000). The data are presented as mean ± standard error (SE)

Sample	Electrolyte	Applied potential (V)	Current (mA)	Mean particle size (μm)	Spread (μm)	Thickness (μm)
E-0.5	MTBS	0.5	5.68	2.30 ± 0.18	1.50 ± 0.27	25.31 ± 1.79
E-1	MTBS	1	9.50	2.06 ± 0.11	1.21 ± 0.17	19.20 ± 0.68
E-2	MTBS	2	19.82	2.86 ± 0.17	2.13 ± 0.28	27.93 ± 2.67
E-5	MTBS	5	45.58	0.92 ± 0.04	0.61 ± 0.06	15.33 ± 1.19
F-0.5	—	0.5	0.50	0.90 ± 0.02	0.43 ± 0.02	2.93 ± 0.39
F-1	—	1	0.76	0.98 ± 0.03	0.45 ± 0.04	4.19 ± 0.26
F-2	—	2	0.96	1.32 ± 0.09	1.19 ± 0.13	8.88 ± 1.10
F-5	—	5	2.21	2.10 ± 0.03	1.10 ± 0.05	15.76 ± 1.19

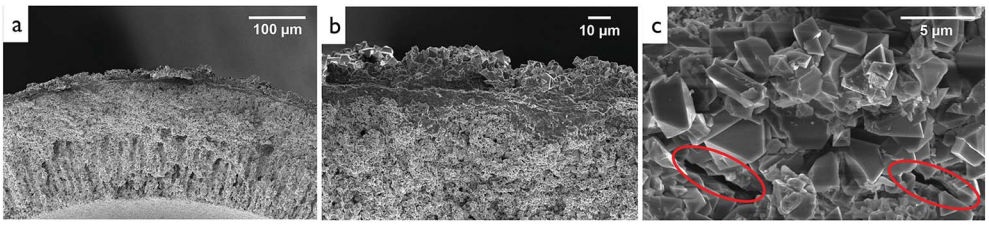

Fig. 2 Formation of Cu-BTC MOF films (E-1). (a and b) Cross-sectional SEM images of the Cu-BTC-coated Cu HFs. (c) The outer surface of the HF. Red circles indicate the cracks present.

with and without the supporting electrolyte are in good agreement with simulated Cu-BTC (Fig. 4(a)), from the study of Zhou (2013) *et al.*, CCDC 943009.[46] Powder XRD patterns ($2\theta = 7$–50°) confirm the crystal structure of the Cu-BTC, indicating the successful synthesis of Cu-BTC films on the Cu HFs. The total weight change (3.5%) between 50 and 800 °C in the TGA analysis corresponds to the thin MOF films on the outer surface of the fiber (Fig. 4(b)). The initial weight loss between 50 and 200 °C (0.7%) is attributed to the residual ethanol, adsorbed water on the surface, and coordinated water molecules in the MOF structure.[47] The TGA results show that the MOF is stable up to 280 °C and the decomposition of the organic ligand, trimesic acid, starts at temperatures higher than 280 °C.

Some MOF formation within the pores of the fiber is also observed, specifically close to the outer surface of the HF (Fig. S2†). Electrochemical reactions occur at the interface between the surface of the working electrode and the solution.[48] Due to the porous nature of the HF, the reaction occurs in the pores as the organic ligand (BTC) solution can diffuse into the pores. The acidity of the BTC solution (pH = 3) can possibly enable the dissolution of the copper ions in the pores while there is a negligible electric potential gradient within the pores driving transport.[15] The BTC molecules can react with these copper ions and form Cu-BTC MOFs in the pores of the HF as well. Dissolution of metal substrates with the combination of the acidity effect and high temperature (higher than 110 °C) has been also reported previously.[32]

3.2 Effect of the supporting electrolyte

Introducing a supporting electrolyte into the synthesis can help to overcome the high electrical resistance of the organic solvent and hence aid reduction of the ohmic drop of the solution. An organic supporting electrolyte, MTBS, is often used in the electrochemical synthesis of MOFs.[49] The release of the copper ions occurs much faster in a supporting electrolyte solution as all the electrical potential drop occurs close to the surface so that the efficiency of the electrochemical MOF powder synthesis is improved.[20] However, in this case we have observed some disadvantages of using a supporting electrolyte based synthesis solution for thin film MOF formation on HFs.

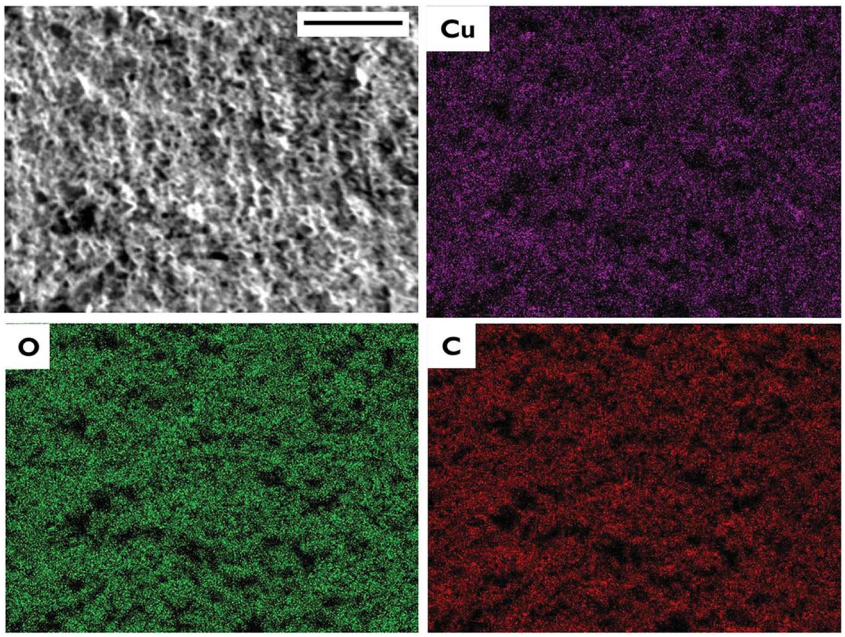

Fig. 3 SEM image of the outer surface of the Cu-BTC-coated Cu HF (F-0.5). EDS map showing copper, oxygen and carbon distribution. Scale bar, 30 μm.

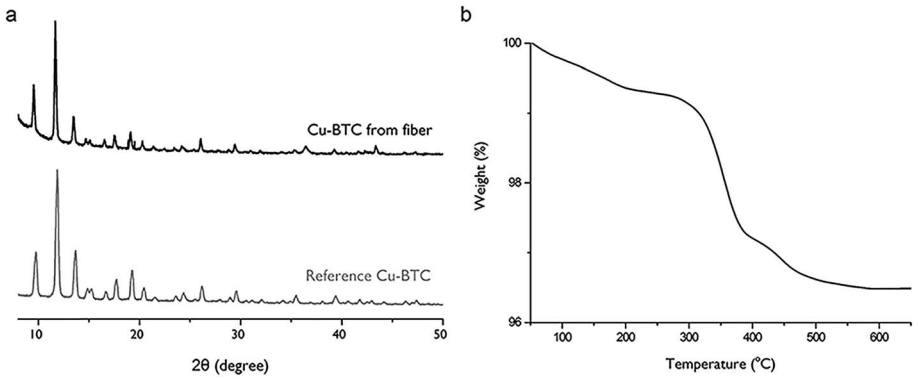

Fig. 4 (a) XRD patterns of the Cu-BTC sample scratched from fibers and simulated Cu-BTC powders (data are taken from the study of Zhou (2013) *et al.*, CCDC 943009, ref. 6). (b) TGA curve of Cu-BTC-coated Cu HFs under continuous nitrogen flow.

Cracks. During the formation of the MOF film, cracks were observed on the copper HF surface as indicated by red circles in Fig. 2(c). The porous copper HF is used both as a substrate and as a metal source for the MOF film synthesis. The growth of the MOF particles on the outer surface of the HF may create internal stress and result in cracks on the substrate, especially when the reaction occurs fast with the help of the supporting electrolyte (MTBS). When the applied potential was increased to 5 V, the effects of the presence of the supporting electrolyte are larger as can be seen in Fig. 5(c and d). The detachment of the MOF increases and the rapid release of the Cu ions causes damage to the Cu HF support. A similar phenomenon on a copper mesh substrate was also reported by Van Assche (2012) and was attributed to the presence of a supporting electrolyte and its effect on kinetics.[18]

Blue solution. During the synthesis with the supporting electrolyte, MTBS, we observed that the reaction solution turned blue within seconds. This color change is characteristic of Cu-BTC MOF powders.[50] This can be the result of both powder synthesis in the liquid bulk and the detachment of the MOF films into the solution. By decreasing the resistance of the organic solvent through introducing MTBS, the faster release of the copper ions promotes the diffusion of these ions into the liquid bulk and synthesis of MOF particles in suspension. This effect of the supporting electrolyte on the reaction kinetics is also promoted the detachment of the MOF films formed on the surface. The copper ions migrating through the MOF films create voids below the MOF films, which results in poor adhesion of the films on the HF, as previously observed.[25] When this

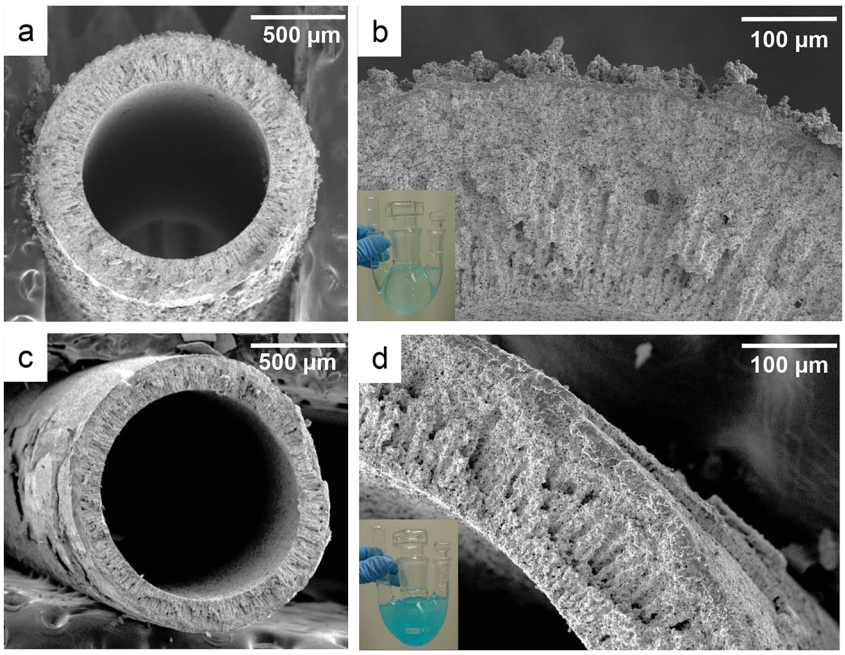

Fig. 5 The effect of applied potential higher than 1 V on the structure of the Cu-BTC-coated Cu HFs. (a) Low and (b) high magnification SEM images of the sample E-2 with the insets showing the solution after synthesis. (c) Low and (d) high magnification SEM images of the sample E-5 with the insets showing the solution after synthesis (contrast and brightness adjustment has been made for (b)–(d)).

phenomenon occurs on a wide area, the MOF films are easily detached from the surface during the synthesis. As can be seen in Fig. 5(a) and (b), large MOF branch-like structures have been observed on the outer surface of the fiber when a potential difference of 2 V was applied in the supporting electrolyte solution. These structures are not physically stable and show poor attachment on the surface of the Cu HF. They can be easily detached from the surface and dispersed in the solution, as can be seen in the corner of Fig. 5(b) where the synthesis solution is partially blue. As the applied potential is increased to 5 V, the synthesis solution showed a deeper blue color (corner of Fig. 5(d)). The branch-like structures formed at this potential completely detached from the surface and damage to the HF support was also observed (Fig. 5(d)). The presence of the supporting electrolyte allows for a very rapid synthesis of the MOF on the surface.

Gas formation. Formation of gas bubbles at the counter electrode has been observed in the presence of a supporting electrolyte at an applied potential higher than 1 V.[51] Hydrogen evolution occurs at high current densities and causes weak adhesion during electrodeposition processes.[52] The detachment of the MOF films into the solution and deformation of the Cu-BTC-coated Cu HF have been observed in E-2V and E-5V (Fig. 5). The presence of a supporting electrolyte increases the current as shown in Table 1, as well as the current densities in the system.

MOF formation on the inner surface. In the samples E-2V and E-5V with the supporting electrolyte some MOF crystals were formed on the inner surface of the HFs (Fig. S3†). These spots with MOFs are not as homogeneous as the outer surface due to the absence of an electric field. As a result, the migration of charged species is absent. The porous copper HF allows BTC to diffuse through the wall of the fiber as well as the access from the bottom of the fiber. The high potential difference near the open end of the fiber can cause dissolution of the Cu ions near this region followed by the formation of MOF particles.

3.3 Electrolyte-free synthesis

By omitting the supporting electrolyte (MTBS) from the synthesis solution more uniform films with smaller particles are obtained on top of the HF (Fig. 6). These smaller particles exhibit better attachment to the Cu HF surface (Fig. 6(b)). Compared to the synthesis with the supporting electrolyte, the same applied potentials now result in substantially lower current values due to the high resistance of the organic solution (Table 1). The low current indicates slower reaction kinetics, evidently favouring more reproducible films. The lack of color change of the synthesis solution during and after the synthesis indicated that the MOF formation primarily occurs on the surface, without substantial detachment from the surface. When MTBS is excluded from the synthesis solution, the cracks and damage on Cu-BTC-coated Cu HFs observed when using the supporting electrolyte solution are not apparent (see Fig. 6).

The electrochemical crystallization occurs at the electrode/solution interface and the limiting factor is the ion transport from the liquid bulk to the electric double layer (EDL).[53] Movement of the ligand species is based on the gradients in the electric potential (migration) and chemical potential (diffusion), and the motion of the bulk fluid. In the absence of stirring the motion of the bulk fluid can be considered minimal and any potential convective contributions be neglected. Therefore, assuming that the mixture is thermodynamically ideal, the net transport of species i can be described *via* the Nernst–Planck equation as:[52]

$$\text{Flux} = \text{diffusion} + \text{electromigration} \quad (1)$$

$$J_i = -D_i \nabla c_i - \frac{z_i F}{R\,T} D_i c_i \nabla \Phi \quad (2)$$

where J_i is the flux of species i in mol m^{-2} s^{-1}, D_i is the diffusion coefficient of species i in m^2 s^{-1}, c_i is the concentration of species i in mol m^{-3}, z_i is the charge number of the species i (dimensionless), F is the Faraday's constant in C mol^{-1}, R is the gas constant in J mol^{-1} K^{-1}, T is the temperature in K, and Φ is the electric potential in V.

In this study, the electroformation of MOF films occurs at the interface between the porous copper working electrode and the synthesis solution. By applying an electric potential, copper ions are released from the surface while BTC molecules diffuse or migrate to the EDL from the bulk. The migration of BTC molecules from the bulk depends on the electric potential gradient in the system. In the supporting electrolyte-free solution, there is a drastic ohmic drop in the solution due to the use of an organic solution, ethanol. This ohmic drop means there is an electric-field in the bulk (potential gradient) and transport of the BTC molecules would be facilitated through both migration and diffusion. Therefore, the BTC transport to the EDL would be enhanced in electrolyte-free synthesis. In addition, a low

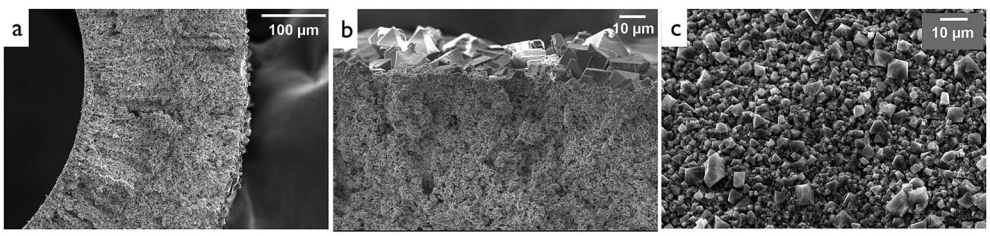

Fig. 6 Formation of Cu-BTC MOF films (F-0.5). (a and b) Cross-sectional SEM images of the Cu-BTC-coated Cu HFs. (c) The outer surface of the HF.

current implies that copper dissociation from the pure copper HF is slow. The combined faster supply of BTC at the EDL surface and the slow and controlled release of the copper at this location results in the formation of thin and homogeneous MOF films comprising small crystals. A similar phenomenon was observed for hydrothermal synthesis of Cu-BTC on an alumina support previously; a low concentration of the precursors was suggested to result in small crystals and controlled layer formation.[54]

Addition of a supporting electrolyte minimizes the electric potential drop in the bulk meaning there is limited contribution from electromigration. With the addition of the electrolyte, nearly all the change in electric potential occurs very close to the electrode surface. The transport of BTC molecules will then be primarily due to diffusion associated with a concentration gradient. Based on the free water diffusion coefficients, Cu^{2+} ions (1.43×10^{-9} m^2 s^{-1}) diffuse faster than the BTC molecules (7.6×10^{-10} m^2 s^{-1}).[35,55] The limited supply of BTC at the electrode will lead to a less controlled film formation. This will become more pronounced when more copper is generated on the surface, *i.e.*, at higher values of the current. When there is a large excess of copper ions, growth of Cu-BTC in the bulk fluid will become more apparent. Combined with the diffusion limitations of BTC, this can also result in a non-uniform concentration distribution around the growing crystals.[53]

Another mechanism that affects the film properties is the adsorption of BTC on the copper HF surface. The presence of a molecular adlayer of BTC molecules, on copper surfaces, was previously reported by Schäfer, 2017.[31] This layer would initiate the first layer of Cu-BTC MOF films. When applying higher potentials, the adlayer thickness would also then increase which explains the thicker MOF films obtained at higher potentials. The presence of the supporting electrolyte may also influence the adsorption of BTC by limiting the transport of BTC to the electrode surface which results in non-homogeneous and non-uniform MOF films.

3.4 Particle size

The particle size histogram, data and corresponding least squares fit are depicted in Fig. 7 for a representative sample synthesized without an electrolyte (and in Fig. S4† for synthesis with a supporting electrolyte). The results of the particle size analysis, including mean particle size and the spread of the MOF crystals and the thickness of the MOF films, are reported in Table 1. The results show that the mean particle size and the spread decrease after removing the supporting electrolyte from the synthesis solution. A slight increase of the particle size with increasing the applied potential can be observed for the experiment without the supporting electrolyte. When a potential higher than 1 V (E-2, E-5) is applied to the copper HF, with the supporting electrolyte, either the MOF films are detached from the surface of the HF or MOF powders are formed in the solution. It can be also seen from the SEM images in Fig. 5(c) and (d) that the HF is damaged at 5 V. The SEM images of this sample show only the films left on the surface after the partial detachment.

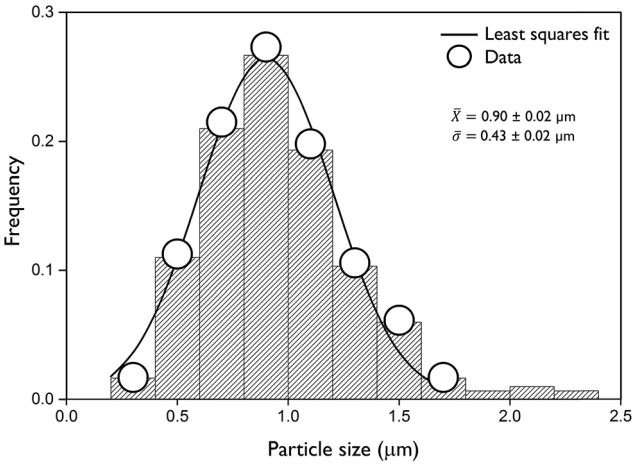

Fig. 7 Gaussian distribution of particle size of sample F-0.5 with least squares fit, along with larger aggregates. Mean particle size ($\bar{X}$) and the spread ($\bar{\sigma}$) values are shown in the graph.

Based on classical nucleation theory it is expected that a higher applied potential will result in smaller crystals.[22] Ameloot (2009) *et al.* observed a decrease in the particle size when increasing the applied potential from 2.5 V to 25 V in a supporting electrolyte system.[17] By increasing the voltage, a higher dissolution rate and higher concentration of copper ions on the surface are obtained, which lead to a higher nucleation rate and smaller crystals.[17] Van Assche (2012) *et al.* also observed the same behavior for film formation in a smaller applied potential range (0.2–4 V) and explained it with the relationship between high current densities and high concentration of metal ions near the surface.[22] However, Joaristi (2012) *et al.* observed that large current densities did not result in a large number of nuclei and small crystals.[19] In this study, we have also observed that lower applied potential and lower current densities (without the supporting electrolyte) lead to smaller crystals. It is important to note that crystal growth is also a function of supersaturation.[56–58] In electrochemical crystallization processes, the extent of supersaturation is directly related to the potential difference between the equilibrium potential and the applied potential, *i.e.*, the overpotential.[53] Overpotential impacts copper oxidation on the copper HF surface. The higher the overpotential, the higher the amount of copper ions released from the surface. In the electrolyte-free synthesis, the overpotential can be considered to be lower *vs.* the case with the supporting electrolyte, because more of the potential drop occurs within the bulk rather than near the surface. Lower supersaturation (or lower overpotential) means slower nucleation and potentially relatively faster crystal growth which can result in larger crystals.[57] However, for the MOF film formation, not only copper oxidation but also the BTC transport to the EDL plays a crucial role. In the electrolyte-free synthesis, the enhanced transport of BTC *via* electromigration and diffusion supplies more BTC to the surface of the nucleus and this evidently contributes to the uniformity of the particle size. As a result, supplying less copper but in a slow and controlled manner along with the enhanced transport of BTC ensures MOF

film formation on the surface with a uniform layer and smaller crystals. In addition, electrochemical adsorption is also another important part of the crystallization.[31,53,59] Nucleation starts with the adsorbed molecules on the surface. More uniform nucleation sites might be created in the electrolyte-free synthesis. With the use of MTBS, there is also an additional chance that the anionic part can be adsorbed on the surface of the copper HF along with BTC molecules. In the supporting electrolyte synthesis, the adlayer of BTC initiates the nucleation process, while the MTBS adsorbed sites cause non-uniformity and a large spread in the particle size of the Cu-BTC crystals. In the electrolyte-free synthesis, nucleation points can be created in a controlled manner which favors the formation of smaller particles in the desired location.

3.5 Thickness

As depicted in Table 1, the thickness of the MOF films increases when a supporting electrolyte is used in the synthesis solution. In the presence of the supporting electrolyte, potential drop occurs primarily near the surface due to smaller resistance in the bulk which indicates higher overpotential than that in electrolyte-free synthesis. When a potential difference is applied, dissociation of the copper starts immediately. This was observed during the synthesis; within seconds of applying a potential, the HF starts to change color to the characteristic blue of Cu-BTC. The activation energy for the crystallization is overcome much faster than that in supporting-electrolyte-free synthesis.[19] These fast kinetics allow the MOF crystals to grow as a thick film because more copper is generated with the help of the high overpotential. Sample E-5V has much thinner MOF films due to the removal of the particles to the solution. This makes it difficult to compare the data with the rest of the samples. The sample E-2V shows agglomerated branch-like MOFs instead of a MOF film. Therefore, the effect of the applied potential on the samples with the supporting electrolyte cannot be fully understood, mainly due to the detachment of the MOF film into the bulk. For applied potentials smaller than 2 V, MOF films were obtained. In the electrolyte-free synthesis, the thickness of the obtained MOF films was decreased. Homogeneous and thin MOF films were obtained, as can be seen in Table 1. When increasing the applied potential, more copper is oxidized and the thickness of the MOF films increased.

MOF particles that separated from the surface turn the synthesis solution blue, which is a characteristic color of Cu-BTC MOFs. The increase in the thickness results in the detachment of the particles from the surface, as can be seen in Fig. 6. After drying the samples, it was observed that some MOF particles were not well attached to the surface and were also removed. As the diffusion limitations control the transport of copper and BTC in the case with the supporting electrolyte, the difference in diffusion coefficients between copper and BTC strongly influences the result. Copper diffuses much faster compared to BTC based on their ionic size (diffusion coefficients), which hinders formation of the MOF near the surface.

Table 1 also shows an increase of the thickness when increasing the applied potential in the electrolyte-free synthesis along with the increase in the overpotential. More copper ions are generated at the surface and all of these copper ions react with the organic linker, BTC, with the increase of the overpotential which results in thicker MOF films. Neither colour change nor detachment was observed for this set of experiments.

3.6 Effect of applied potential

The effect of the applied potential in the range of 0.5–5 V *vs.* SHE is discussed for solutions with and without the supporting electrolyte. As is depicted in Fig. 8 and 9, and is reported in Table 1, a comparison between electrolyte-free and with-electrolyte samples shows that the standard error (SE) and

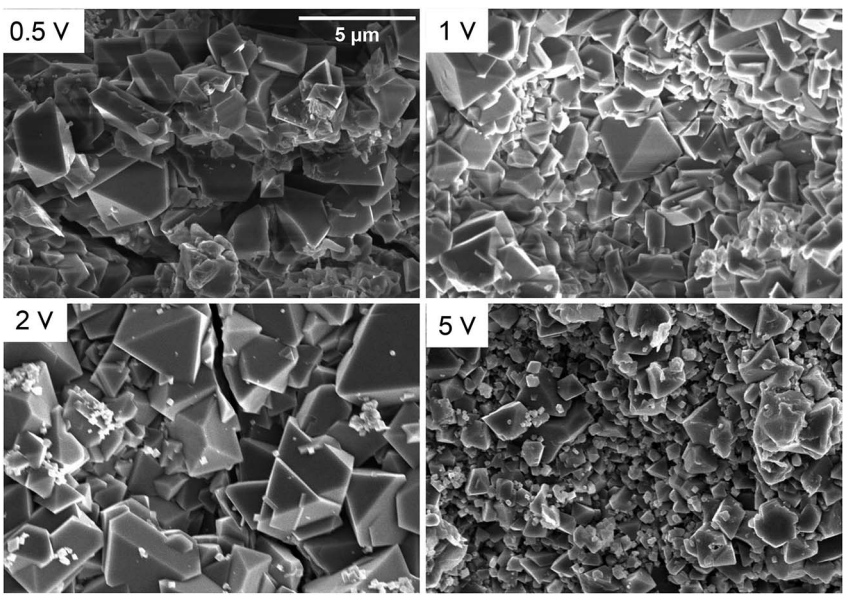

Fig. 8 SEM images of the outer surface of the Cu-BTC-coated Cu HFs: E-0.5, E-1, E-2, and E-5.

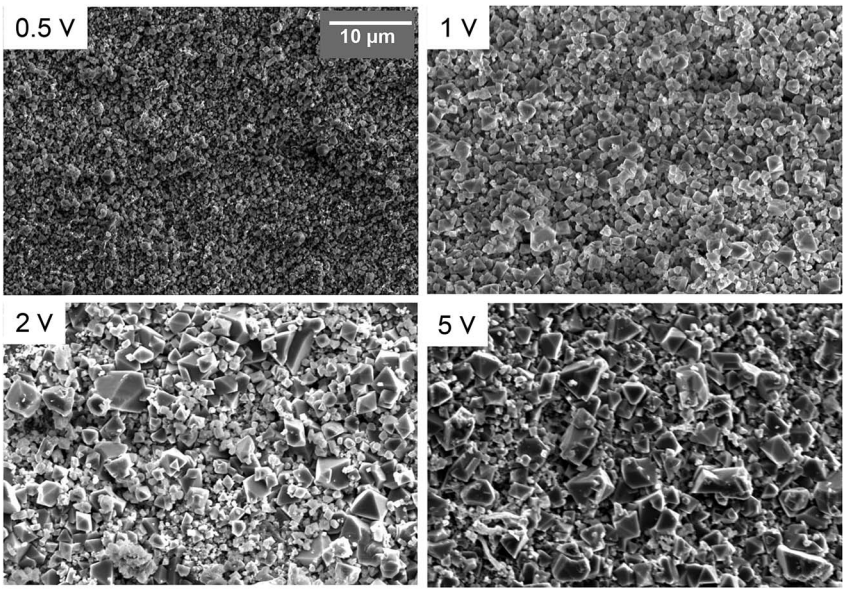

Fig. 9 SEM images of the outer surface of the Cu-BTC-coated Cu HFs: F-0.5, F-1, F-2, and F-5.

spread values decreased drastically in supporting electrolyte-free solutions, indicating that more uniform MOF particles with relatively narrower distributions are formed. The mean particle size increases with increasing potential. Based on the nucleation theory, higher applied potentials should result in smaller crystals.[17] By increasing the voltage, a higher dissolution rate and higher concentration of copper ions on the surface are obtained, which lead to a higher nucleation rate and smaller crystals.[60] However, the porous nature of the copper HF electrode also allows more Cu ions to be released to the surface and react with the organic linker ions even at lower voltages. The study of Joaristi (2012) *et al.* also has showed theoretically that only 0.124 V is necessary to overcome the nucleation activation energy of 71.6 kJ mol^{-1} for Cu-BTC MOFs.[19] All the applied potentials in this study are above this nucleation activation energy barrier. As also described above, overpotential as the replacement of the supersaturation is the key factor to explain the electrocrystallization of MOF films. When increasing the applied potential, the overpotential is also increased. The critical Cu ion concentration for the MOF formation is reached rapidly and this allows crystals to grow for a longer time.

The current values were decreased by a factor of more than 10 times when omitting the supporting electrolyte from the synthesis. The current is directly proportional to the oxidation at the anode so the current and time give a qualitative estimate of the crystal growth and the film thickness. In the electrolyte-free synthesis, the thickness increases in direct proportion to the applied potential. In the case of using the supporting electrolyte, when the thicknesses of the synthesized films are increased, the attachment of the films to the surface also becomes weaker and results in easier removal from the surface to the bulk which ultimately results in thinner and discontinuous films in the analysis. The current is lower due to the resistance of the organic linker solution in a water–ethanol mixture. Most of the applied potential is used to overcome the ohmic drop of the solution.[19] Higher current usually refers to higher reaction efficiency and yield.[18,19] It is crucial to note the distinct difference between MOF powder synthesis and film formation.[17,18,22,24,31,35,61–63] Our results show that a decrease in the current is not detrimental but can result in the formation of more uniform films. Cu-BTC-coated Cu HFs prepared without the supporting electrolyte are promising candidates for future applications such as gas separation or catalysis.

We found that an applied potential of only 0.5 V *vs.* SHE for both electrolyte-free and electrolyte containing systems was sufficient to obtain thin MOF films. In the earlier studies of electroforming MOF films, the applied potential has been varied between 2.5 and 25 V.[17] However, this was done using a two-electrode system instead of a three-electrode cell. In a two-electrode cell, it is not possible to control the exact applied potential to the surface of the working electrode which can limit the reproducibility of the experiments. A third electrode is needed to standardize the potential with respect to the reference electrode so that the potential on the working electrode can be controlled.[48,52] Second, to synthesize MOF powders, higher applied potentials are necessary as the goal is to oxidize the anode and release metal ions into the bulk where MOF particles are formed. To electrochemically form MOF films, the anode must be partially oxidized and not damaged, so that the dissociated metal ions do not migrate to the bulk and stay near the surface in order to form MOF films. By increasing the potential, the migration of metal ions away from the surface is also promoted. As mentioned above, the efficiency of the MOF film fabrication is not directly related to the high concentration of metal ions, high potential–current, *etc.* A precise control of the kinetics of the reaction and crystallization is more important. To support our results, it is necessary to repeat that only 0.124 V is theoretically necessary to overcome the nucleation activation energy. Cyclic voltammetry studies have also shown that the copper oxidized at 0.18 V in the presence of

trimesic acid, which is in reasonable agreement with theoretical calculations.[31]

4 Conclusions

In this paper, we have prepared Cu-BTC MOF coated HFs by a partial anodic dissolution electrochemical route. We have used porous copper HFs as the anode, metal source and support simultaneously for the fabrication of the MOF films. The successful formation of Cu-BTC MOF films onto porous copper HFs is confirmed by SEM, EDS, XRD and TGA. The effects of the supporting electrolyte and applied potential on the electrosynthesis of MOF films have been quantified. A supporting electrolyte is typically used to increase the conductivity of the synthesis solution and enhance the electron transfer during electrochemical synthesis of MOF powders. However, we found that the use of a supporting electrolyte for MOF film formation has numerous disadvantages. It results in cracks on the MOF films, detachment of MOF films, the formation of MOF particles in the bulk, and gas formation at the counter electrode. By increasing the conductivity of the synthesis solution, controlling the electroformation of MOF films on the fiber becomes more challenging.

Alternatively, by using an electrolyte-free solution and lower potential differences we have obtained thinner and more reproducible Cu-BTC films. The potential drop primarily occurs near the electrode surface with a supporting electrolyte, while without the supporting electrolyte (electrolyte-free) this potential drop is mainly in the bulk. The lower potential drop at the electrode surface in the electrolyte-free case lowers the rate of copper ion generation while also enhancing the transport of BTC, the slower diffusing molecule, to the surface for a higher degree of control of the MOF film formation. In order to obtain thin, dense and uniform MOF films, the control of kinetics and synthesis location is crucial compared to the bulk synthesis. The applied potential changes the overpotential in the system, which is related to the release of copper ions available for the synthesis. Therefore, an increase in the particle size and film thickness has been observed for higher applied potentials. Utilization of electrochemical synthesis for MOF formation on a HF support is a straightforward and fast synthesis compared to the conventional methods *e.g.* solvothermal synthesis.[42] The synthesized HFs in our work are promising for numerous applications, in particular gas separation[64,65] or catalysis[66,67] due to their high surface areas, porosity and scalability for wide-scale use. This work represents an important first step towards utilizing these HFs, after further work on improving the adhesion and mechanical properties.

Conflicts of interest

There are no conflicts to declare.

Acknowledgements

The authors acknowledge the contribution of Fleur Sebek (University of Twente) to this work and the technical support of the Photo Catalytic Synthesis (PCS) group from University of Twente.

References

1 H. Furukawa, N. Ko, Y. B. Go, N. Aratani, S. B. Choi, E. Choi, A. O. Yazaydin, R. Q. Snurr, M. O'Keeffe, J. Kim and O. M. Yaghi, *Science*, 2010, **329**, 424–428.
2 H. Furukawa, K. E. Cordova, M. O'Keeffe and O. M. Yaghi, *Science*, 2013, **341**, 1230444.
3 H. Li, M. Eddaoudi, M. O'Keeffe and O. M. Yaghi, *Nature*, 1999, **402**, 276–279.
4 S. K. Elsaidi, M. H. Mohamed, D. Banerjee and P. K. Thallapally, *Coord. Chem. Rev.*, 2018, **358**, 125–152.
5 D. Zhao, D. J. Timmons, D. Yuan and H.-C. Zhou, *Acc. Chem. Res.*, 2011, **44**, 123–133.
6 A. Schneemann, S. Henke, I. Schwedler and R. A. Fischer, *ChemPhysChem*, 2014, **15**, 823–839.
7 H. Li, K. Wang, Y. Sun, C. T. Lollar, J. Li and H.-C. Zhou, *Mater. Today*, 2018, **21**, 108–121.
8 L. E. Kreno, K. Leong, O. K. Farha, M. Allendorf, R. P. Van Duyne and J. T. Hupp, *Chem. Rev.*, 2012, **112**, 1105–1125.
9 M. D. Allendorf, A. Schwartzberg, V. Stavila and A. A. Talin, *Chem.–Eur. J.*, 2011, **17**, 11372–11388.
10 T. Granato, F. Testa and R. Olivo, *Microporous Mesoporous Mater.*, 2012, **153**, 236–246.
11 R. Jin, Z. Bian, J. Li, M. Ding and L. Gao, *Dalton Trans.*, 2013, **42**, 3936.
12 Z. Y. Yeo, S.-P. Chai, P. W. Zhu and A. R. Mohamed, *RSC Adv.*, 2014, **4**, 54322–54334.
13 J. Cookney, W. Ogieglo, P. Hrabanek, I. Vankelecom, V. Fila and N. E. Benes, *Chem. Commun.*, 2014, **50**, 11698–11700.
14 R. Makiura, S. Motoyama, Y. Umemura, H. Yamanaka, O. Sakata and H. Kitagawa, *Nat. Mater.*, 2010, **9**, 565–571.
15 W.-J. Li, M. Tu, R. Cao and R. A. Fischer, *J. Mater. Chem. A*, 2016, **4**, 12356–12369.
16 U. Mueller, M. Schubert, F. Teich, H. Puetter, K. Schierle-Arndt and J. Pastré, *J. Mater. Chem.*, 2006, **16**, 626–636.
17 R. Ameloot, L. Stappers, J. Fransaer, L. Alaerts, B. F. Sels and D. E. De Vos, *Chem. Mater.*, 2009, **21**, 2580–2582.
18 T. R. C. Van Assche, G. Desmet, R. Ameloot, D. E. De Vos, H. Terryn and J. F. M. Denayer, *Microporous Mesoporous Mater.*, 2012, **158**, 209–213.
19 A. Martinez Joaristi, J. Juan-Alcañiz, P. Serra-Crespo, F. Kapteijn and J. Gascon, *Cryst. Growth Des.*, 2012, **12**, 3489–3498.
20 M. Rubio-Martinez, C. Avci-Camur, A. W. Thornton, I. Imaz, D. Maspoch and M. R. Hill, *Chem. Soc. Rev.*, 2017, **46**, 3453–3480.
21 I. Buchan, M. R. Ryder and J.-C. Tan, *Cryst. Growth Des.*, 2015, **15**, 1991–1999.
22 T. R. C. Van Assche, N. Campagnol, T. Muselle, H. Terryn, J. Fransaer and J. F. M. Denayer, *Microporous Mesoporous Mater.*, 2016, **224**, 302–310.
23 S. D. Worrall, H. Mann, A. Rogers, M. A. Bissett, M. P. Attfield and R. A. W. Dryfe, *Electrochim. Acta*, 2015, **197**, 228–240.

24 P. Schäfer, M. A. van der Veen and K. F. Domke, *Chem. Commun.*, 2016, **52**, 4722–4725.
25 N. Campagnol, T. Van Assche, L. Stappers, J. F. M. Denayer, K. Binnemans, D. E. De Vos and J. Fransaer, *ECS Trans.*, 2014, **61**, 25–40.
26 M. Li, M. Dincă and M. Dinc, *J. Am. Chem. Soc.*, 2011, **133**, 12926–12929.
27 M. Li and M. Dincă, *Chem. Sci.*, 2014, **5**, 107–111.
28 R. Ameloot, L. Pandey, M. Van Der Auweraer, L. Alaerts, B. F. Sels and D. E. De Vos, *Chem. Commun.*, 2010, **46**, 3735.
29 H. Zhu, H. Liu, I. Zhitomirsky and S. Zhu, *Mater. Lett.*, 2015, **142**, 19–22.
30 I. Hod, W. Bury, D. M. Karlin, P. Deria, C.-W. Kung, M. J. Katz, M. So, B. Klahr, D. Jin, Y.-W. Chung, T. W. Odom, O. K. Farha and J. T. Hupp, *Adv. Mater.*, 2014, **26**, 6295–6300.
31 P. Schäfer, A. Lalitha, P. Sebastian, S. K. Meena, J. Feliu, M. Sulpizi, M. A. van der Veen and K. F. Domke, *J. Electroanal. Chem.*, 2017, **793**, 226–234.
32 N. Campagnol, T. Van Assche, T. Boudewijns, J. Denayer, K. Binnemans, D. De Vos and J. Fransaer, *J. Mater. Chem. A*, 2013, **1**, 5827.
33 M. Hartmann, S. Kunz, D. Himsl, O. Tangermann, S. Ernst and A. Wagener, *Langmuir*, 2008, **24**, 8634–8642.
34 U. Mueller, H. Puetter, M. Hesse, M. Schubert, H. Wessel, J. Huff and M. Guzmann, *US Pat.*, US 7968739 B2, 2011.
35 N. Campagnol, T. R. C. Van Assche, M. Li, L. Stappers, M. Dincă, J. F. M. Denayer, K. Binnemans, D. E. De Vos and J. Fransaer, *J. Mater. Chem. A*, 2016, **4**, 3914–3925.
36 S. Yadnum, J. Roche, E. Lebraud, P. Négrier, P. Garrigue, D. Bradshaw, C. Warakulwit, J. Limtrakul and A. Kuhn, *Angew. Chem., Int. Ed.*, 2014, **53**, 4001–4005.
37 Y. Zhang, I. H. Musselman, J. P. Ferraris and K. J. Balkus, *J. Membr. Sci.*, 2008, **313**, 170–181.
38 J. Dechnik, C. J. Sumby and C. Janiak, *Cryst. Growth Des.*, 2017, **17**, 4467–4488.
39 M. Etxeberria-Benavides, O. David, T. Johnson, M. M. Łozińska, A. Orsi, P. A. Wright, S. Mastel, R. Hillenbrand, F. Kapteijn and J. Gascon, *J. Membr. Sci.*, 2018, **550**, 198–207.
40 A. J. Brown, N. A. Brunelli, K. Eum, F. Rashidi, J. R. Johnson, W. J. Koros, C. W. Jones and S. Nair, *Science*, 2014, **345**, 72–75.
41 A. M. Marti, W. Wickramanayake, G. Dahe, A. Sekizkardes, T. L. Bank, D. P. Hopkinson and S. R. Venna, *ACS Appl. Mater. Interfaces*, 2017, **9**, 5678–5682.
42 N. Abdullah, M. A. Rahman, M. H. Dzarfan Othman, J. Jaafar and A. A. Aziz, *J. Membr. Sci.*, 2018, **563**, 162–174.
43 R. Kas, K. K. Hummadi, R. Kortlever, P. de Wit, A. Milbrat, M. W. J. Luiten-Olieman, N. E. Benes, M. T. M. Koper and G. Mul, *Nat. Commun.*, 2016, **7**, 10748.
44 T. J. Smith and K. J. Stevenson, in *Handbook of Electrochemistry*, ed. C. G. Zoski, Elsevier, 2007, pp. 73–110.
45 C. A. Schneider, W. S. Rasband and K. W. Eliceiri, *Nat. Methods*, 2012, **9**, 671–675.
46 A. A. Yakovenko, J. H. Reibenspies, N. Bhuvanesh and H. C. Zhou, *J. Appl. Crystallogr.*, 2013, **46**, 346–353.
47 W. W. Lestari, I. D. Winarni and F. Rahmawati, *IOP Conf. Ser.: Mater. Sci. Eng.*, 2017, **172**, 012064.
48 M. Atobe, in *Fundamentals and Applications of Organic Electrochemistry*, ed. T. Fuchigami, S. Inagi and M. Atobe, John Wiley & Sons, Ltd, Weinheim, 1st edn, 2014, pp. 1–10.
49 H. Al-Kutubi, J. Gascon, E. J. R. Sudhölter and L. Rassaei, *ChemElectroChem*, 2015, **2**, 462–474.
50 R. Senthil Kumar, S. Senthil Kumar and M. Anbu Kulandainathan, *Microporous Mesoporous Mater.*, 2013, **168**, 57–64.
51 P. Atkins and J. de Paula, *Physical Chemistry*, Oxford University Press, Oxford, 10th edn, 2014.
52 A. J. Bard and L. R. Faulkner, *Electrochemical Methods, Fundamentals and Applications*, Wiley, New York, 2nd edn, 2001.
53 A. Milchev, *Electrocrystallization Fundamentals of Nucleation and Growth*, Kluwer Academic Publishers, Dordrecht, 2002.
54 J. Gascon, S. Aguado and F. Kapteijn, *Microporous Mesoporous Mater.*, 2008, **113**, 132–138.
55 R. L. Hershey and W. Fereday, *Laboratory Experiments to Evaluate Matrix Diffusion of Dissolved Organic Carbon Carbon-14 in Southern Nevada Fractured-Rock Aquifers*, Las Vegas, 2016.
56 S. Dodds, J. A. Wood and P. A. Charpentier, *Ind. Eng. Chem. Res.*, 2007, **46**, 8009–8017.
57 H. Grön, A. Borissova and K. J. K. Roberts, *Ind. Eng. Chem. Res.*, 2003, **42**, 198–206.
58 T. Vetter, M. Iggland, D. R. Ochsenbein, F. S. Hänseler and M. Mazzotti, *Cryst. Growth Des.*, 2013, **13**, 4890–4905.
59 J. Mostany and B. Scharifker, in *Encyclopedia of Electrochemistry*, ed. A. J. Bard, Wiley-VCH Verlag GmbH & Co. KGaA, Weinheim, Germany, 2007, pp. 512–540.
60 W.-J. Li, J. Lü, S.-Y. Gao, Q.-H. Li and R. Cao, *J. Mater. Chem. A*, 2014, **2**, 19473–19478.
61 L.-L. Jiang, X. Zeng, M. Li, M.-Q. Wang, T.-Y. Su, X.-C. Tian and J. Tang, *RSC Adv.*, 2017, **7**, 9316–9320.
62 S. Sachdeva, M. R. Venkatesh, B. El Mansouri, J. Wei, A. Bossche, F. Kapteijn, G. Q. Zhang, J. Gascon, L. C. P. M. de Smet and E. J. R. Sudhölter, *Small*, 2017, **13**, 1604150.
63 L. Ji, J. Wang, K. Wu and N. Yang, *Adv. Funct. Mater.*, 2018, **28**, 1706961.
64 Y. Mao, J. Li, W. Cao, Y. Ying, L. Sun and X. Peng, *ACS Appl. Mater. Interfaces*, 2014, **6**, 4473–4479.
65 Y. Mao, L. Shi, H. Huang, W. Cao, J. Li, L. Sun, X. Jin and X. Peng, *Chem. Commun.*, 2013, **49**, 5666–5668.
66 A. Sachse, R. Ameloot, B. Coq, F. Fajula, B. Coasne, D. De Vos and A. Galarneau, *Chem. Commun.*, 2012, **48**, 4749.
67 J. Lee, O. K. Farha, J. Roberts, K. A. Scheidt, S. T. Nguyen and J. T. Hupp, *Chem. Soc. Rev.*, 2009, **38**, 1450.

